Refinements to the Utah−Washington Mechanism of Electron Capture Dissociation
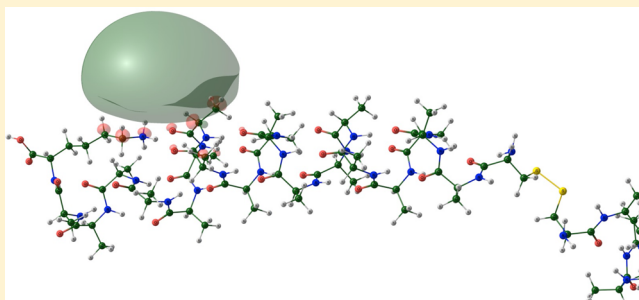
Iwona Anusiewicz,[†] Piotr Skurski,[†] and Jack Simons*[,‡]

[†]Department of Chemistry, University of Gdańsk, Wita Stwosza 63, 80-308 Gdańsk, Poland

[‡]Chemistry Department and Henry Eyring Center for Theoretical Chemistry, University of Utah, Salt Lake City, Utah 84112, United States

S *Supporting Information*

ABSTRACT: Ab initio electronic structure calculations on a rather geometrically constrained doubly positivley charged parent peptide ion are combined with experimental data from others on three similar ions to refine understanding of the mechanistic steps in the Utah−Washington model of electron-capture and electron-transfer dissociation. The primary new findings are that (i) the electron need not first attach to a Rydberg orbital and subsequently be extracted by an SS σ^* or amide π^* orbital (rather, it can be guided directly into the SS σ^* or amide π^* orbital by the Rydberg orbital) and (ii) Coulomb and dipole potentials within the parent ion alter both the electron binding strengths and radial ranges of Rydberg orbitals located on the positively charged sites, which, in turn, alters the ranges over which the electron can be guided. These same potentials, when evaluated at disulfide or backbone amide sites, determine which disulfide σ^* and amide π^* orbitals are and are not susceptible to electron attachment leading to SS and N−C_α bond cleavage. Additional experiments on the same parent ions discussed here are proposed to further test and refine the UW model.

1. INTRODUCTION

In electron-transfer dissociation[1−5] (ETD) mass spectrometry, an electron from an anion donor is transferred to a multiply positively charged gas-phase peptide. In electron-capture dissociation[6−9] (ECD), it is a free electron having low kinetic energy that attaches to the peptide. ECD and ETD are relatively new yet extremely promising analytical techniques that have been found to generate significantly higher backbone cleavage fractions than collisional or infrared activation techniques, while doing so with great specificity (i.e., in peptides, primarily N−C_α and S−S bonds are cleaved). Why these bonds cleave and why they do throughout such a large fraction of the backbone has been the focus of much of our theoretical work in this area.[10] The central issues in these studies have been

1. identifying where in the peptide (and into what kind of orbital and with what cross-section) the excess electron is initially bound,
2. characterizing to where, over what distances, and at what rates the electron may subsequently migrate within the peptide, and
3. understanding how the excess electron's presence causes specific bonds (e.g., backbone N−C_α bonds are found to preferentially break) to be cleaved and with what relative probabilities.

A. Review of the Utah−Washington Mechanism. As a result of our earlier studies and those of the Turecek and others,[11−39] a mechanistic picture referred to as the Utah− Washington (UW) mechanism has evolved within which it is the attachment of an electron to a backbone amide π^* or disulfide σ^* orbital that causes N−C_α or SS bond cleavage. Many aspects of the UW mechanism and comparisons with alternative mechanistic proposals have recently been comprehensively reviewed[40] by Turecek and Julian, so only the most essential points will be summarized here.

Because electron attachment to amide π^* or disulfide σ^* orbitals in the absence of stabilizing influences (e.g., solvation or intramolecular electrostatic potentials) is ca. 2.0 or 1.0 eV endothermic,[41] respectively, not all such orbitals are amenable to electron attachment. Those that are amenable are determined by the local intramolecular electrostatic potentials stabilizing the orbitals (if the potential is not strong enough, electron attachment cannot occur) arising largely from Coulomb potentials of the positively charged sites and dipole potentials created by polar functional groups within the peptide. So, within the UW model, for ECD, only amide π^*

or disulfide σ^* orbitals along the peptide backbone that experience Coulomb and dipole stabilization exceeding 2.0 or 1.0 eV, respectively, can attach an electron. In ETD, the stabilization must be even larger; it must exceed the electron binding energy of the anion donor by 2.0 or 1.0 eV.

Another component of the UW model deals with how the ECD or ETD electron gets to the amide π^* or disulfide σ^* orbital. The most frequently discussed two-step version of the model posits that Rydberg orbitals located on the peptide's positively charged sites act as antennas to which the ECD or ETD electron initially attaches. The electron subsequently transfers from such a Rydberg orbital into an amenable amide π^* or disulfide σ^* orbital over distances related to the radial size of that Rydberg orbital. Within this version of the UW model, the amide π^* or disulfide σ^* orbital's stabilization must be larger than 2.0 or 1.0 eV, respectively, because extra energy is required to extract the electron from the Rydberg orbital. That is, the stabilization must exceed 2.0 or 1.0 eV plus the electron binding energy of the Rydberg orbital.
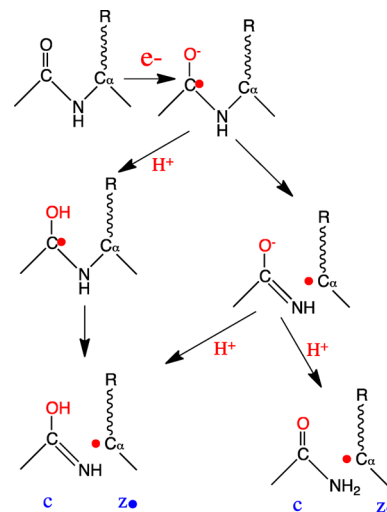
An alternative to two-step Rydberg electron attachment followed by electron extraction has also been suggested as a modification to the UW model. In the alternative[42] one-step variant, Rydberg orbitals on a positive site act to shuttle or guide (through orbital overlap) the ECD or ETD electron into the amide π^* or disulfide σ^* orbital, but the electron does not become bound to the Rydberg orbital. As a result, the Coulomb and dipole stabilization at the amide π^* or disulfide σ^* orbital does not have to overcome the electron binding energy of the Rydberg orbital, whereas in the two-step model it does. The one-step variant of the UW model was explored after Turecek and others[43,44] suggested that dipole potentials within parent ions can act to guide electrons to sites near the positive regions of the dipole. In the present paper, experimental data are used to argue against the two-step version of the UW mechanism and in favor of the one-step alternative.

Once the electron enters an SS σ^* orbital, cleavage of the associated disulfide bond is prompt because the $\sigma^2\sigma^{*1}$ anionic electronic state is repulsive. If the electron enters an amide π^* orbital, cleavage of the associated $N-C_\alpha$ bond can occur by surmounting a barrier that is much smaller than the barrier needed to homolytically cleave this $N-C_\alpha$ bond in the absence of the excess electron. The route by which such $N-C_\alpha$ cleavage is thought to occur once the electron enters the amide π^* orbital is shown in Scheme 1.

After the electron attaches to the amide π^* orbital, the $N-C_\alpha$ bond is weakened because cleaving it allows a new $C-N$ π bond to form; this is why the barrier to cleavage is reduced.

There are two possible pathways outlined in Scheme 1. In one, the $^-O-C{=}NH$ anion is formed first and then abstracts a proton to form either the enol-imine (bottom left in Scheme 1) or the more stable amide (bottom right). The proton can be abstracted either from the N-terminal or C-terminal direction (likely from the most proximal site of low proton affinity). Alternatively, it is possible that the proton is abstracted prior to cleavage of the $N-C_\alpha$ bond, in which case formation of the enol-imine would be favored. Experimental infrared spectroscopic evidence[34] suggested that the amide is formed once the reaction has proceeded to completion, but this is not conclusive proof that the proton is transferred after $N-C_\alpha$ bond cleavage because the enol-imine, if formed first, could subsequently rearrange to the thermodynamically more stable amide. In fact, a recent experimental and theoretical study[45] of (GLGGK +2H)$^{2+}$ doubly charged peptides concluded that, once the

Scheme 1

$^-O-C{=}NH$ unit is formed, proton transfer from a nearby protonated site occurs with a lower energy barrier than for $N-C_\alpha$ bond cleavage, thus favoring the pathway in which $N-C_\alpha$ bond cleavage occurs after proton transfer.

Within the one-step guiding variant of the UW mechanism, the ECD or ETD process occurs as described above except the electron does not have to first attach to a Rydberg orbital and subsequently be extracted by the SS σ^* or amide π^* orbital. Instead, the Rydberg orbitals act to guide the electron to the SS σ^* or amide π^* orbital where initial electron attachment then occurs.

B. Peptide Whose Data Can Test and Refine the UW Mechanism. The high degree of backbone and side-chain flexibility that exists in most gas-phase peptides has limited our ability to put the UW mechanism to stringent tests. The problem is that the energetic (e.g., Coulomb and dipole potentials at amide π^* and SS σ^* orbitals) and geometric (e.g., interatomic distances) data required to implement the UW model vary widely as a flexible peptide undergoes thermal motion. However, the peptides (AcCA$_N$K+H)$_2^{2+}$ are believed to be more geometrically constrained because they consist of a central cystine unit containing a disulfide bond that connects to the N-termini of two α-helices composed of N alanines with each helix having a protonated lysine at its C-terminus. By combining experimental data on the ECD fragmentation of such peptides with our computational data on similar species, in this paper, we show evidence that supports the one-step variant of the UW model.

To illustrate some of the structural features important to this study, in Figure 1 we show two views of an $N = 20$ peptide that is similar to (AcCA$_N$K+H)$_2^{2+}$ but contains a slightly different disulfide linkage; we refer to this peptide as (H-LysAla$_{20}$-S)$_2^{2+}$. The techniques used to obtain this structure are detailed in section 2 of this paper. In both views, the right portion of the figure is cut off so we can focus on the left half; no information is lost because the structure has symmetry around the S−S bond site.

The top of Figure 1 shows the minimum-energy geometry including the disulfide linkage and the lowest-energy Rydberg orbital on the −NH$_3^+$ group of the left Lys site. This view is intended to show that the Ala$_N$ units adopt α-helical structures and that the Lys unit is involved in hydrogen bonds but not to the C=O groups nearest the C-termini. The bottom Figure 1

Distances from Lys N atom to various C=O O atoms:
O_1=6.6 Å; O_2=8.6 Å; O_3=5.6 Å; O_4=3.7 Å; O_5=6.1 Å; O_6=4.8 Å; O_7=2.8 Å;
O_8=2.4 Å; O_9=5.6 Å; O_{10}=6.7 Å; O_{11}=7.1 Å; O_{12}=9.1 Å; O_{13}=11.0 Å; O_{14}=11.9 Å
Distances from Lys N atom to various C=O C atoms:
C_1=6.5 Å; C_2=7.5 Å; C_3=5.1 Å; C_4=3.5 Å; C_5=5.6 Å; C_6=4.9 Å; C_7=3.3 Å;
C_8=3.9 Å; C_9=6.3 Å; C_{10}=7.6 Å; C_{11}=8.3 Å; C_{12}=10.1 Å; C_{13}=12.0 Å; C_{14}=13.1 Å
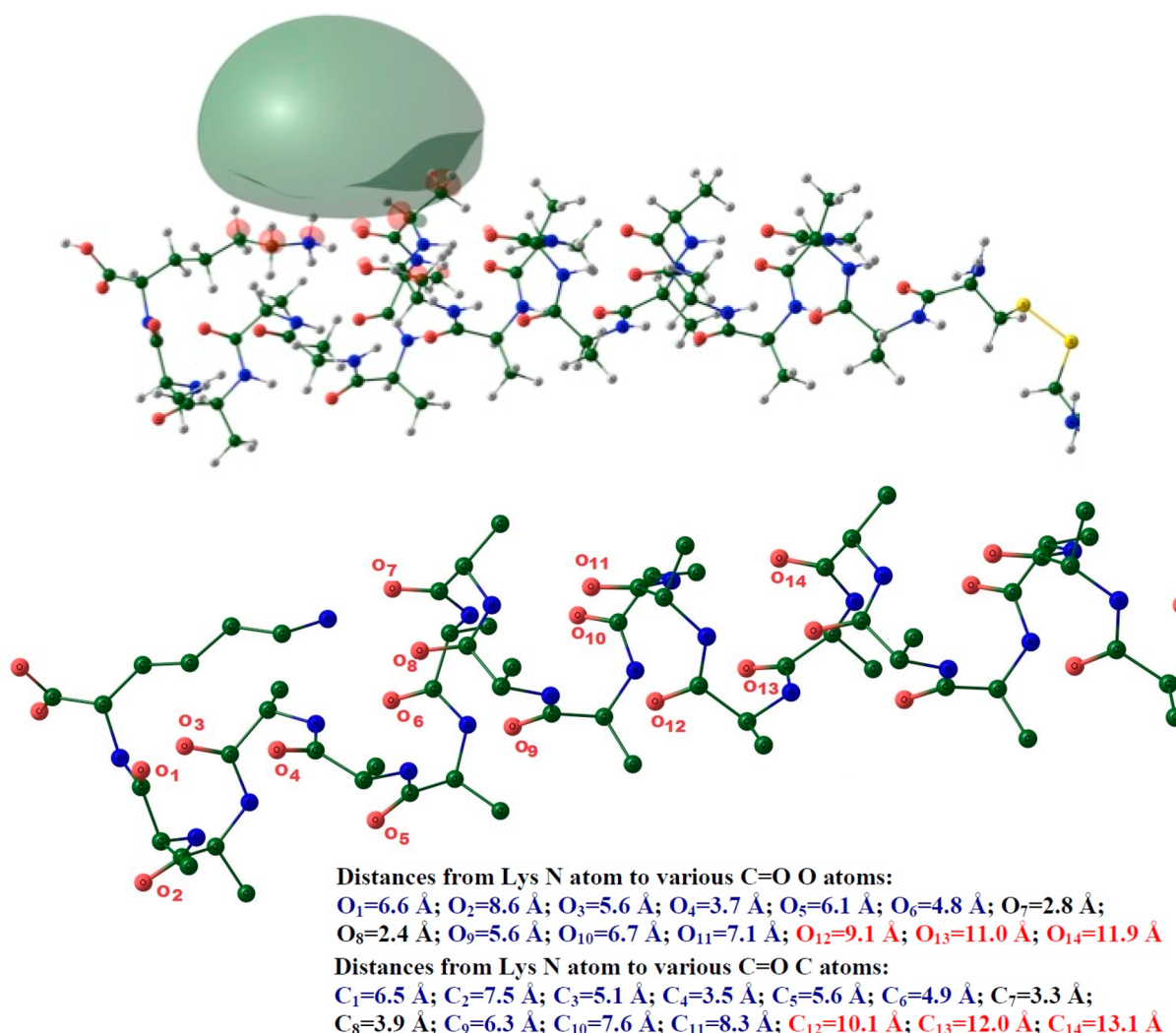
Figure 1. The minimum-energy structure of $(H\text{-}LysAla_{20}\text{-}S)_2^{2+}$ showing the 3s Rydberg orbital on the left protonated Lys site (top). Close-up of left C-terminus of the same structure (with all H atoms not shown) showing distances from the C-terminal Lys' N atom to nearby carbonyl O and C atoms (bottom).

focuses on the C-terminus of the left helix and on its charged Lys site, the terminal COOH, and the C=O units close to the Lys. In this view the H atoms are not shown so that distances from the charged Lys' N atom to several nearby carbonyl O and C atoms can be illustrated as these distances play important roles in estimating the Coulomb potential at the backbone amide sites.

C. Electrostatic Potential within the Peptide. The electrostatic potential at various locations within these $(H\text{-}LysAla_N\text{-}S)_2^{2+}$ polypeptides (e.g., near backbone amide π^* or SS σ^* orbitals) has been shown to consist of two dominant contributions. First, there are Coulomb potentials

$$C = \frac{-14.4 \text{ eV Å}}{R_1 \text{ (Å)}} + \frac{-14.4 \text{ eV Å}}{R_2 \text{ (Å)}} \qquad (1)$$

generated by the two charged Lys sites. This potential at any amide π^* or disulfide σ^* orbital depends on the distances R_1 and R_2 from the two charged sites to that orbital.

The second potential is the dipole potential arising from the polarity of the backbone amine and carbonyl groups forming peptide bonds. Others have shown[46,47] that the dipole moment of Ala_N α-helices can be accurately represented by an array of q

= +1/2 charges located near each backbone N atom and q = −1/2 charges located near each backbone carbonyl O atom. This collection of partial charges can also be represented by a quasi-linear array of +1/2 and −1/2 charges along the α-helix's symmetry axis with the partial charges spaced by 1.5 Å. Each such pair of +1/2 and −1/2 charges produces a dipole moment of 3.5 D. In Figure 2, we show the +1 Lys charge and the +1/2 and −1/2 fractional (±q) charges on several atoms on the left α-helix of the $N = 20$ peptide. Notice that, because the Ala_N
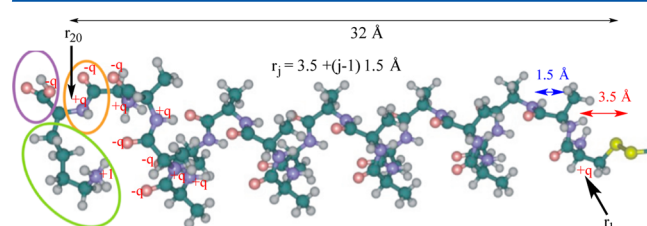

Figure 2. Close-up view of the left C-terminus of $(H\text{-}LysAla_{20}\text{-}S)_2^{2+}$ for $N = 20$ showing locations of partial ±1/2 charges and how distances from various partial charges to the midpoint of the SS bond are estimated.

helices are connected at their N-termini to the disulfide linkage, the positive end of each Ala_N helix's dipole moment is directed toward the SS bond; the negative end of each dipole points toward the Lys unit. This orientation is important to emphasize because, as we show later, it plays a key role in stabilizing the SS σ^* orbital while destabilizing Rydberg orbitals on the Lys site.

Also, in Figure 2 we show how we estimate distances (i) from the midpoint of the SS bond to the nearest positive partial charge (3.5 Å), (ii) along the helix axis from one positive partial charge to the next (1.5 Å), and (iii) from the midpoint of the SS bond to the farthest positive partial charge (32 Å for the $N = 20$ peptide). Finally, notice that each of the $+q/-q$ dipoles located along the backbones of the α-helices has its positive end directed toward the SS bond.

Clearly, the structural rigidity of the $(H\text{-}LysAla_N\text{-}S)_2^{2+}$ systems, combined with knowledge of how to describe the internal electrostatic potential with reasonable accuracy makes these peptides excellent candidates for further testing the UW model's predictions. After discussing our computational methods in section 2, section 3 shows results of using geometry data and internal electrostatic potential estimates that allow us to use the experimentally observed disulfide and $N-C_\alpha$ bond cleavage intensities on $(AcCA_NK+H)_2^{2+}$ to further refine the UW model. The refinements thus arrived at are summarized in section 4.

2. METHODS

The geometry optimization of the $(H\text{-}LysAla_{20}\text{-}S)_2^{2+}$ peptide was undertaken using the PM6 semiempirical method.[48,49] The resulting optimized structure shown in Figure 1, is similar to that found earlier by Hudgins et al.[50] for $(AcCA_{15}K+H)_2^{2+}$ and, through molecular modeling and ion-mobility studies, by Hudgins and Jarrold[51] for AcA_NLysH^+ for $N > 6$ and for noncovalently linked $(AcA_{19}LysH)_2^{2+}$ (see Figure 8b in ref 51). The similarity among these structures arises in that they all have Ala-based α-helices, their C-terminal protonated Lys units bend backward to form hydrogen bonds with nearby C=O groups, and the two α-helices are aligned in a near-linear orientation. However, it is important to notice (see Figure 1 as well as Figure 6a,b of ref 51) that the protonated Lys units are hydrogen bonded not to the most C-terminal Ala's C=O groups but to C=O groups several Ala units from the C-terminus. It is also useful to note that the ion mobility data of ref 51 suggest that the quasi-linear structure (rather than containing antiparallel helices or more disordered) is energetically favored. Of course, the ion mobility experiments cannot distinguish among structures that differ only in how the charged Lys site is hydrogen bonded to the α-helix's C=O groups. The structure shown in Figure 1 is predicted to have the lowest energy, but other structures with the Lys hydrogen bonded to different nearby C=O units may have energies that could be accessed in the laboratory formation of the parent ions. Therefore, an ensemble of kinetically trapped (because the ionic hydrogen bonds connecting the charged Lys to nearby C=O groups structures are quite strong) structures having the charged Lys hydrogen bonded to any of the C=O groups labeled 1 through 8 in Figure 1 could exist in the experimental samples whose ECD data are discussed here. Nevertheless, we feel confident in using the system depicted in Figure 1 as representative of the ECD experiments on $(AcCA_NK+H)_2^{2+}$ while also taking into consideration the possibility that the charged Lys need not be hydrogen bonded only to the C=O sites labeled 7 and 8 in Figure 1.

For describing the Rydberg orbitals, extra diffuse functions were added to the nitrogen atoms of both Lys residues. We used six-term even-tempered[52] sp sets that share exponent values with a geometric progression ratio of 3.2,[53] and we started to build up the exponents of these extra diffuse functions from the lowest exponent of the same symmetry included in the 4-31+G basis set[54−58] of nitrogen. As a consequence, we achieved lowest sp exponents of $2.104455354 \times 10^{-4}$. All calculations were performed with the Gaussian09 program.[59]

3. RESULTS

A. Coulomb and Dipole Potentials along the Peptide Backbone. Earlier,[60] we examined the effects of internal Coulomb and dipole potentials on the SS σ^* orbital of the $(H\text{-}LysAla_N\text{-}S)_2^{2+}$ systems. Here, we extend this analysis to describe how these internal potentials alter the energies of amide π^* orbitals and the energies and radial sizes of Rydberg orbitals centered on the charged Lys sites. Both effects play key roles in developing the enhancements to the UW mechanism proposed here.

First, we briefly review our findings relative to the SS σ^* orbital. In Figure 3, we show energy profiles[60] for stretching the central S−S bond in the $N = 20$ species without and with an electron attached to the SS σ^* orbital.
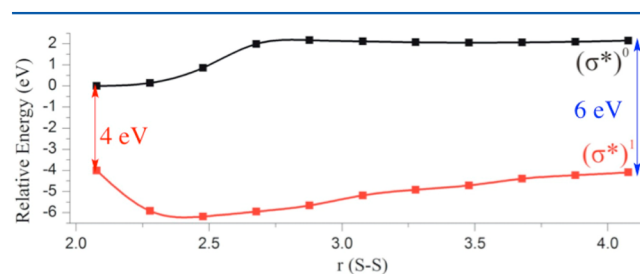

Figure 3. Energy profiles for stretching the S−S bond in $(H\text{-}LysAla_{20}\text{-}S)_2^{2+}$ in the absence of an attached electron (top, black) and with an electron attached to the SS σ^* orbital (bottom, red) (reprinted from ref 60).

The two curves shown in Figure 3 have been interpreted[60] as follows:

1. It is know from electron scattering experiments[41] that, near the equilibrium bond length of the SS bond, it is ca. 1 eV endothermic to vertically attach an electron to the SS σ^* orbital. However, Figure 3 suggests that it is 4 eV exothermic to attach an electron to the SS σ^* orbital in our system, so something generates 5 eV of stabilization at the disulfide site.

2. At extended distances where the SS bond is broken, the SS σ^*-attached state lies ca. 6 eV below the parent dication. The electron affinity of an aliphatic radical R−S$^\bullet$ is expected to be ca. 1 eV, so again the electron-attached state is stabilized by ca. 5 eV.

3. The origin of the 5 eV stabilization of the SS σ^*-attached state was postulated[60] to be a combination of (i) 0.5 eV of stabilization arising from the Coulomb potential from each of the two protonated Lys sites and (ii) ca. 2 eV of stabilization from dipole interaction with each of the two Ala_N helices' dipoles as we now explain.

Using the SS-to-Lys distance of 32 Å (Figure 2a), eq 1 for the Coulomb potential tells us that $14.4/32 = 0.45$ eV of

stabilization could indeed come from each of the two protonated Lys sites, thus providing a total Coulomb stabilization of nearly 1 eV for the SS σ^*-attached state. The remaining 4 eV of stabilization was shown[60] to arise from the two helices' dipole potentials. As mentioned earlier, this potential D can be described[46,47] as arising from the sum of the SS σ^* orbital's interaction with each of the $+1/2$ and $-1/2$ partial (q) charges distributed in a quasi-linear fashion along the axis of the backbone

$$
\begin{aligned}
D &= \frac{-\frac{1}{2}14.4}{3.5} + \frac{\frac{1}{2}14.4}{5.0} + \frac{-\frac{1}{2}14.4}{5.0} + \frac{\frac{1}{2}14.4}{6.5} + \dots + \frac{-\frac{1}{2}14.4}{30.5} \\
&\quad + \frac{\frac{1}{2}14.4}{32} + \frac{-\frac{1}{2}14.4}{32} \\
&= -2.06 + 1.44 - 1.44 + 1.11 - 1.11 + \dots + 0.23 - 0.23 \\
&= -2.06 \text{ eV}
\end{aligned}
\tag{2}
$$

and twice 2.06 eV is reasonably close to the 4 eV of stabilization suggested in Figure 3.

Notice that in eq 2 the distance from the midpoint of the SS bond to the nearest C═O centered $-1/2$ charge (5 Å) is taken to be the same as the distance to the second-nearest NH centered $+1/2$ charge (5 Å). This does not mean that these C═O and NH groups reside at the same point in space. It is simply a reflection of the fact that the α-helical structure aligns the N microdipoles in a manner that causes these distances along the helix's symmetry axis (as well as distances from the SS bond to subsequent C═O and NH pairs) to be nearly identical. As a result, the total potential can be well approximated as the interaction of the SS σ^* orbital with only the nearest partial charge (i.e., the $+1/2$ charge on the nearest NH group)

$$
D = \frac{-\frac{1}{2}14.4}{3.5} = -2.06 \text{ eV}
\tag{3}
$$

Also notice that the $-1/2$ charge on the 20th amino acid's C═O group (at $R = 32$ Å) is counteracted by a $+1/2$ charge representing the $-OH$ group attached to this same C atom (i.e., at the C-terminal COOH group).

B. Internal Electrostatic Potentials on the Protonated Lys Sites Alter the Rydberg Orbitals' Binding Energies and Radial Ranges. As discussed earlier, the charged Lys sites have Rydberg orbitals that are posited in the UW model to initially bind (or guide) the ECD or ETD electron. As we now demonstrate, the electron binding strength of such an orbital is altered by the electrostatic potentials generated by the two α helix dipoles and by the second charged Lys. Getting these binding strengths correct is important because the two-step variant of the UW model requires that they be overcome if an electron is to transfer from such a Rydberg orbital to an amide π^* or SS σ^* orbital.

Earlier work[61] has shown that a protonated primary amine (e.g., a protonated Lys site) has an electron binding energy of 3.5 eV or more when an electron is attached to its lowest-energy orbital (e.g., the 3s-like orbital shown in Figure 1). However, our calculated binding energy for the 3s Rydberg orbital in the full $N = 20$ (H-LysAla$_{20}$-S)$_2^{2+}$ dication is only 1.5 eV. This suggests that the electrostatic potential exerted on this Lys site by the nearby α-helix, the more distant α-helix, and the other charged Lys acts to destabilize this $n = 3$ Lys Rydberg orbital by ca. 2 eV. It is well-known[62,63] that complexation or solvation of charged sites can significantly reduce the electron

binding energies of associated Rydberg orbitals. However, here, for the first time, we make use of this fact to suggest enhancements to the UW model using the role these binding strengths play to differentiate between the two-step and one-step variants.

The other charged Lys is ca. 64 Å away and acts to stabilize the Rydberg orbital by 14.4/64 = 0.23 eV. The more distant α-helix, if represented by a quasi-linear chain of 20 dipoles as used to arrive at eqs 2 and 3, has as its closest partial charge a $-1/2$ charge on its S atom ca. 32 Å from the Rydberg orbital. This partial charge representing the more distant α-helix's influence generates a potential of $1/2 \times 14.4/32 = 0.23$ eV, which acts to destabilize the Rydberg orbital. So, the other Lys charge and the more distant α-helix dipole cancel from which we conclude that the proximal α-helix's electrostatic potential is likely the main source of the ca. 2 eV destabilization of the 3s Rydberg orbital observed in our calculation.

There are two important consequences of the destabilization of the protonated Lys' Rydberg orbitals. First, lowering the electron binding energies of these orbitals means that amide π^* or disulfide σ^* orbitals do not have to overcome as high an energy barrier to extract an electron in the two-step variant of the UW mechanism. Second, Rydberg orbitals having lower electron binding energies will consequently have larger radial extents that determine the distances over which these orbitals can transfer an electron.

It is conventional to express the electron binding energies (BE) of Rydberg orbitals of a given angular momentum (here we will focus on s orbitals to illustrate) in terms of a principal quantum number n and a so-called quantum defect δ as

$$
\text{BE}(n) = \frac{13.6 \text{ eV}}{(n-\delta)^2}
\tag{4}
$$

Because the $n = 3$ Rydberg orbital of the destabilized Lys site has a BE of only 1.5 eV, eq 4 gives a quantum defect near zero. This allows us to estimate the BE values for higher Rydberg energy levels by using eq 4 with $n > 3$ and $\delta = 0$, as shown in Table 1.

Table 1. Protonanted Lys's Rydberg Orbitals' Ranges and Electron Binding Energies (BE) for Principal Quantum Numbers Ranging from 3 through 6

quantum no. n	orbital range (Å)	BE (eV)
3	3.5–7.7	1.50
4	6.3–12.7	0.85
5	10.2–19.0	0.54
6	14.9–26.3	0.38

Also shown in Table 1 are the radial ranges characterizing the $n = 3$ through $n = 6$ Rydberg orbitals of the destabilized protonated Lys site. The average value $\langle r \rangle$ of the distance of the electron from the nitrogen nucleus of the Lys is given in terms of n as

$$
\langle r \rangle = 0.529n(n + 1/2)\text{Å}
\tag{5}
$$

and the mean-square displacement about $\langle r \rangle$, which we use to define the range $\langle r \rangle \pm T$ of the Rydberg orbital, is expressed as

$$
T = \sqrt{[\langle r^2 \rangle - \langle r \rangle^2]} = 0.529n\sqrt{\frac{n + 1/2}{2}} \text{ Å}
\tag{6}
$$

In Figure 4 we show plots of the radial electron densities as functions of distance from the Lys nitrogen atom for $n = 3$
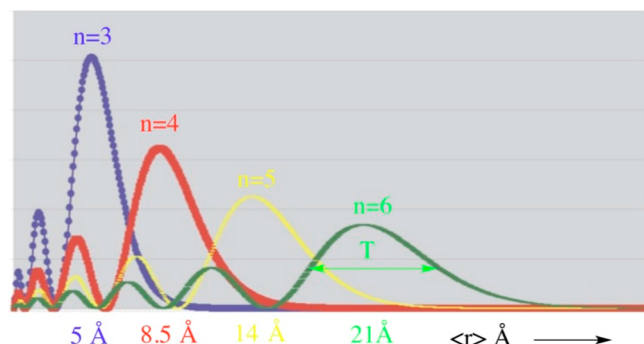

Figure 4. Radial densities of $n = 3$ through $n = 6$ Rydberg orbitals having binding energies as given in Table 1.

through $n = 6$ Rydberg orbitals having the BEs and radial extents given in Table 1.

In Figure 5, we show the left half of the $(H\text{-}LysAla_{20}\text{-}S)_2^{2+}$ system below which we indicate the ranges of the $n = 3$ through $n = 6$ Rydberg orbitals.
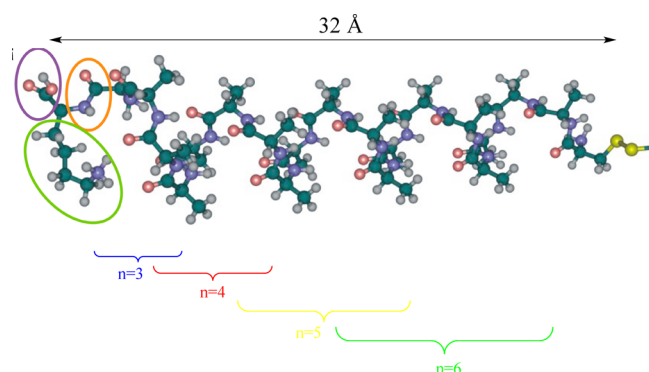

Figure 5. Left half of $(H\text{-}LysAla_{20}\text{-}S)_2^{2+}$ showing the radial ranges of the $n = 3$, 4, 5, and 6 Rydberg orbitals on the protonated Lys.

C. Electrostatic Potentials Also Determine Amide π^* Orbitals' Binding Energies. Above the internal electrostatic potential of $(H\text{-}LysAla_{20}\text{-}S)_2^{2+}$ was shown to stabilize the disulfide σ^* orbital by ca. 5 eV and to destabilize the $n = 3$ Rydberg orbital on each protonated Lys by ca. 2 eV. In the Supporting Information, we make use of analogs of eqs 1 and 2 to describe the Coulomb and dipole potentials near amide π^* orbitals along the backbone. There, we show that the total Coulomb plus dipole potential experienced at the kth amide π^* orbital (with $k = 1$ corresponding to the site closest to the SS) consists of a stabilizing Coulomb term (see eq S3) and a destabilizing dipole term (see eq S4). In Table 2, we summarize these two contributions for R values of 18, 24, and 32 (corresponding to $N = 10$, 15, and 20) and for $k = 1$ and for k corresponding to the middle of the right α-helix.

The main observations to make about how these potentials vary with R and with k are as follows:

1. For small values of k (i.e., near the disulfide linkage), the total potential is repulsive, suggesting that amide π^* orbitals in this region are not able to attach an ECD or ETD electron because a stabilizing potential in excess of 2.0 eV is needed to allow attachment.

Table 2. Coulomb and Dipole Potentials (eV) at the Amide π^* Orbital Closest to the SS Site ($k = 1$) and the Middle Amide π^* Orbital for $(H\text{-}LysAla_N\text{-}S)_2^{2+}$ Having $N = 10$, 15, and 20

R (Å)/N	$k = 1$	$k = $ middle
32/20	$C = -0.14$	$C = -0.80$
	$D = +0.92$	$D = +0.26$
24/15	$C = -0.26$	$C = -1.10$
	$D = +0.86$	$D = 0.27$
18/10	$C = -0.48$	$C = -1.56$
	$D = +0.80$	$D = 0.33$

2. Moving toward the C-terminus in the α-helix as k increases, the total potential becomes attractive, but even at the midpoint, it does not reach the critical 2.0 eV.

3. Therefore, the trends displayed in Table 2 suggest that amide π^* orbitals of $(H\text{-}LysAla_N\text{-}S)_2^{2+}$ are not sufficiently (i.e., >2.0 eV) stabilized to bind an electron except when the orbital is near a charged Lys site, which is where the Coulomb potential dominates.

D. Connections among Electrostatic Potentials at SS and Amide Sites, Rydberg Orbitals' Radial Ranges, and ECD Fragment-Ion Abundances. *a. Data Favoring the One-Step UW Variant.* As described in Scheme 1, cleavage of an $N\text{-}C_\alpha$ bond gives rise to fragments denoted c and z. Because the $(AcCA_NK+H)_2^{2+}$ parent ions are doubly charged, the fragment c or z ions will be singly charged. Moreover, when $N\text{-}C_\alpha$ bonds near one of the Lys sites are cleaved, the proton that eventually transfers to form the closed-shell c and open-shell z fragments (Scheme 1) most likely is extracted from this nearby charged Lys site. For this reason, the c fragments are produced as singly charged ions and the z fragments as neutrals. So, electron attachment to the C-terminal amide π^* orbital of site 1 in Figure 1 followed by $N\text{-}C_\alpha$ bond cleavage would produce fragment ions denoted c_{N+1} if the peptide contains N Alas. Attachment to sites 2 through 4 produces c_N, c_{N-1}, and c_{N-2}, and so on.

To distinguish between the one- and two-step variants, we recall that the UW model posits that amide π^* orbitals have to be within ca. 7.2 Å of a charged site to be stabilized by 2.0 eV and we note (Figure 4) that the $n = 3$ and $n = 4$ Rydberg orbitals span such distances. If an amide π^* orbital were <u>also</u> required to be able to extract an electron from an $n = 3$ or $n = 4$ Rydberg orbital (whose electron binding energies are ca. 1.5 and 0.85 eV, respectively), the amide π^* orbital would have to be stabilized in excess of 2.85 eV for $n = 4$ (3.5 eV for $n = 3$). This would require the orbital to be within 5 Å for $n = 4$ (4 Å for $n = 3$) of a charged site. In Table 3, we summarize which of the amide π^* orbitals lie within 7.2, 5, or 4 Å of a protonated Lys's nitrogen atom according to Figure 1.

To illustrate how we can use the information in Table 3 to distinguish between the one- and two-step variants, we note that amide sites 1 and 2 (i.e., nearest the C-termini) do not meet the 5 Å criterion. So, if amide π^* binding energies in excess of 2.85 eV were necessary, as in the two-step variant of the UW model, we would expect little c_N and c_{N+1} fragment ion abundance, but c_{N-1}, c_{N-2}, through c_{N-6} ions should be present (column 3 of Table 3). Let us see what the experimental data tells us.

In Figure 6 we show mass spectra[50] of ions obtained by ECD-induced fragmentation of $(AcCA_NK+H)_2^{2+}$ for $N = 10$, 15, and 20 (top to bottom) with ion intensity appearing on the

Table 3. Does an Amide π^* Orbital at a Given Site Lie Closer than 7.2, 5, or 4 Å to a Lys' Nitrogen Atom in Figure 1 (Using ± 0.5 Å as Uncertainty)?

amide site relative to the C-terminus	amide O or N atom within 7.2 $\pm$ 0.5 Å?	amide O or N atom within 5 $\pm$ 0.5 Å?	amide O or N atom within 4 $\pm$ 0.5 Å?	amide O or N atom inside 3.5 Å?
1	yes	no	no	
2	yes	no	no	
3	yes	yes	no	
4	yes	yes	yes	
5	yes	yes	no	
6	yes	yes	no	
7	yes	yes	yes	yes
8	yes	yes	yes	yes
9	yes	no	no	
10	yes	no	no	
11	yes	no	no	
12 and higher	no	no	no	

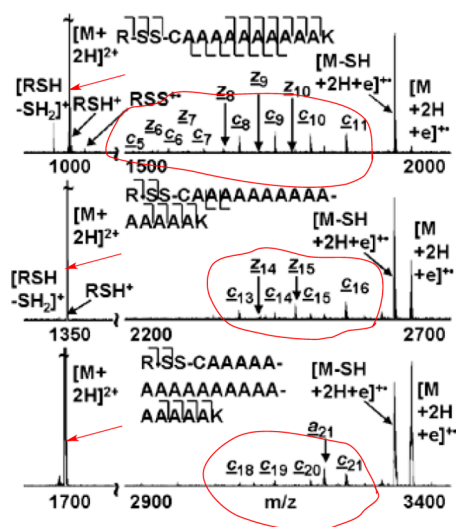**Figure 6.** Mass spectral ion intensities for fragmentation of $(AcCA_NK+H)_2{}^{2+}$ under ECD conditions for $N = 10$ (top), 15 (middle), and 20 (bottom). The red arrows point to the peak arising from fragmentation of the SS bond, and the red circles focus attention on the fragments arising from cleaving $N-C_\alpha$ bonds close to the C termini. Adapted from ref 50.

vertical axis and ion mass-to-charge ratio on the horizontal axis. In all three data sets, the c_N and c_{N+1} ions occur and with abundances similar to those of c_{N-1} and c_{N-2} ions. These findings are inconsistent with the two-step variant of the UW model if the structural data in Figure 1 are to be believed (recall from our earlier discussion that structures similar to those in Figure 1, including its hydrogen bonding motif, are consistent with the ion-mobility and molecular modeling data reported in ref 51).

Next, we note that amide sites 1 and 2 do lie within 7.2 Å of the protonated Lys (column 2 of Table 3), so they have Coulomb stabilization in excess of 2 eV. This means that sites 1 and 2 are capable of binding an electron even if they are not capable of extracting an electron from an $n = 3$ or $n = 4$ Rydberg orbital on the Lys. Hence, the fact that c_N and c_{N+1} ions are formed (and in abundances comparable to those of c_{N-1} and c_{N-2} ions) suggests that extracting the electron from

the Lys Rydberg orbital is not necessary, thus inclining us toward the one-step variant of the UW model.

The data in Figure 6 also support another aspect of the UW model as applied to the structural data of Figure 1 summarized in Table 3. The fifth column of Table 3 tells us that only amide sites 7 and 8 have their π^* orbitals closer than 3.5 Å to the Lys's nitrogen atom. So, these sites are Coulomb stabilized by more than 4 eV and thus have electron binding energies in excess of 2 eV, which is much more than that necessary to extract an electron from an $n = 3$ or $n = 4$ Rydberg orbital. Nevertheless, these sites produce little, if any corresponding c_{N-5} or c_{N-6} fragment ions (Figure 6) even though they are closest to the Lys site and are very powerful electron binders. In Figure 4, we see that the Rydberg orbitals have very little density within ca. 3.5 Å; most of their density resides at larger distances. Within the UW model, this means that the Rydberg orbitals cannot effectively overlap with[64] and thus guide electrons into amide π^* orbitals if the amide site is closer than ca. 3.5 Å. So, the absence of fragmentation arising from amide sites 7 and 8 is consistent with this aspect of the UW mechanism and with the structural data in Figure 1.

However, as noted in section 2, we must also consider the possibility that hydrogen bonding motifs differing from that shown in Figure 1 (where hydrogen bonds to C=O groups labeled 7 and 8 are shown) may also be present in the experiment's parent ions even if the structure shown in Figure 1 is lower in energy. For example, the charged Lys might be hydrogen bonded to any of the C=O groups labeled 1 through 6. It is therefore useful to examine ECD data also from ref 50 on disulfide linked dimers $(AcCA_{10}\text{-}NH_2+Na)_2{}^{2+}$ similar to those whose ECD fragmentation patterns are shown in Figure 6 but with the C-termini amidated. Such ions are thought[65] to have Ala_{10} α-helices with the Na^+ ions bound to the C-terminal $-NH_2$ sites. For such structures, the locations of the positive charges and the distances to various amide C=O groups can more reliably be estimated because the charges do not reside on a flexible Lys side chain. In particular, the charged sites are most likely near where Figure 1 positions the C-terminal $-COOH$ groups (which are replaced by $-CONH_2Na^+$ groups). The c_k fragment ions observed (Figure 3 of ref 50) under ECD cleavage of $(AcCA_{10}\text{-}NH_2+Na)_2{}^{2+}$ include c_{11}, c_{10}, c_9, and c_8 in abundances similar to those shown (Figure 6) for $(AcCA_{10}K+H)_2{}^{2+}$. From Figure 1, one can estimate the distances from the $-NH_2Na^+$ charged site to the C=O groups corresponding to fragments c_{11} though c_8. Although C=O site 1 (producing c_{11}) may well be within 4−5 Å of the Na^+ charge, sites 3 and 4 (producing c_9 and c_8) are not. On the other hand, sites 1 through 4 would be within 7.2 Å of the Na^+. So, the observation of $N-C_\alpha$ bond cleavage from sites 1 through 4 in $(AcCA_{10}\text{-}NH_2+Na)_2{}^{2+}$ is more consistent with the one-step variant (which requires proximity of ca. 7.2 Å or less) than with the two-step variant (which requires proximity of ca. 5 Å or less).

To summarize, the one-step variant of the UW mechanism appears to be in line with the experimental data of Figure 6 if the structural data shown in Figure 1 is reliable. In this view, the charged sites can serve to attract the ECD electron (or ETD donor anion), but the electron does not attach to a Rydberg orbital on the charged site. Rather, these Rydberg orbitals act to guide the electron into any amide π^* or SS σ^* orbital that is sufficiently stabilized. The guiding is generated through the overlap of the Rydberg orbital with the π^* or σ^* orbital, and the distance between the charged site and the π^* or σ^* orbital determines which Rydberg orbital does the guiding.

b. Proposal for How ETD Fragmentation of the Disulfide Bond Could Be Used to Further Refine the UW Model. Another notable feature of the data sets shown in Figure 6 is that the peak relating to S—S bond cleavage is very intense. This is consistent with the UW model because

1. The SS σ^* orbital lies within or very close to the radial range of the $n = 6$ Rydberg orbitals on either Lys site (Figures 4 and 5), so these Rydberg orbitals could guide the ECD electron into the SS σ^* orbital.

2. The 4 eV electron binding energy of the SS σ^* orbital is much higher than that of any of the amide π^* orbitals. This may play a role in determining why the intensity of the fragment ion derived from SS bond cleavage is so much more intense than any of the peaks corresponding to c_k ion formation.

Unfortunately, these observations do not offer insight into whether the two-step or one-step variant of the UW model is favored because the SS σ^* orbital is stabilized by more than enough to allow it to extract an electron from the $n = 6$ Rydberg orbital within whose radial range it lies. However, if the experiments were carried out using ETD rather than ECD conditions, useful information could be obtained. For example, if a donor anion having an electron binding energy of ca. 0.6 eV were used, and *if* initial electron attachment to a Rydberg orbital were necessary, then only $n = 3$ and $n = 4$ Rydberg orbitals could be populated; $n = 5$ and $n = 6$ orbitals could not because their electron binding energies do not exceed that of the donor anion (Table 1). Because $n = 3$ and $n = 4$ Rydberg orbitals do not have the radial range to transfer an electron from the charged Lys to the SS σ^* orbital (at least for $(AcCA_{20}K+H)_2^{2+}$ and probably for $(AcCA_{15}K+H)_2^{2+}$), no SS fragmentation should occur. On the other hand, *if* initial electron attachment to a Rydberg orbital is not necessary, the $n = 6$ Rydberg orbitals could still act to guide the ETD electron into the (stabilized) SS σ^* orbital (whose electron binding energy exceeds that of the donor) and thus cause SS bond cleavage. We therefore suggest that such ETD experiments on $(AcCA_NK+H)_2^{2+}$ ions be carried out.

4. SUMMARY

The four new conclusions reached in this paper are the following:

1. If an amide π^* orbital had to be stabilized in excess of 2.0 eV by an amount needed to extract an electron from an $n = 3$ or $n = 4$ Rydberg orbital (ca. 1.5 or 0.85 eV), it would have to reside within ca. 5 or 4 Å of a charged site. The experimental c_k fragment ion abundance data do not suggest that this is the case, which argues in favor of the Rydberg orbitals serving to guide the electron to the amide π^* orbitals rather than requiring extraction of the electron.

2. The electrostatic potentials act to destabilize by ca. 2 eV (and radially extend) the Rydberg orbitals on the two charged Lys sites of $(H-LysAla_{20}-S)_2^{2+}$; this alters the distances over which these orbitals can guide an ECD or ETD electron.

3. Backbone amide π^* orbitals near the disulfide bond are destabilized, but, as one moves toward either charged Lys site, the π^* orbitals become stabilized (mainly through the Coulomb potential from the nearest charged Lys).

4. The Coulomb stabilization of amide π^* orbitals near a C-terminus is not a simple function of the distance this

orbital is from the C-terminus because the protonated Lys is involved in hydrogen bonds to carbonyl O atoms several residues from that closest to the C-terminus.

Conclusions summarized below derived from earlier work on the UW model include:

5. Coulomb and dipole potentials produce strong stabilization (>5 eV for $(H-LysAla_{20}-S)_2^{2+}$) at the disulfide bond site, with eqs S3 and S4 providing a way to estimate these two potentials. For species containing α-helices (or other strongly dipolar units), the dipole potentials can contribute substantially to the stabilization. Coulomb stabilization is always present for positively charged parent ions.

6. Because electron attachment to amide π^* orbitals requires at least 2.0 eV of stabilization, such orbitals must reside within ca. 7.2 Å of a charged Lys site to generate c_K fragment ions.

Finally, we also suggested experiments (i.e., ETD on $(AcCA_NK+H)_2^{2+}$ looking for SS bond cleavage) whose data could allow us to even further improve the UW model.

■ ASSOCIATED CONTENT

⬡ Supporting Information

Depiction discussion of right α-helix structure. This material is available free of charge via the Internet at http://pubs.acs.org.

■ AUTHOR INFORMATION

Corresponding Author
*J. Simons: e-mail, simons@chem.utah.edu.

Notes
The authors declare no competing financial interest.

■ ACKNOWLEDGMENTS

■ REFERENCES

(1) Syka, J. E. P.; Coon, J. J.; Schroeder, M. J.; Shabanowitz, J.; Hunt, D. F. Peptide and protein sequence analysis by electron transfer dissociation mass spectrometry. *Proc. Natl. Acad. Sci.* **2004**, *101*, 9528–9533.

(2) Coon, J. J.; Syka, J. E. P.; Schwartz, J. C.; Shabanowitz, J.; Hunt, D. F. Anion dependence in the partitioning between proton and electron transfer in ion/ion reactions. *Int. J. Mass Spectrom.* **2004**, *236*, 33–42.

(3) Pitteri, S. J.; Chrisman, P. A.; McLuckey, S. A. Electron-transfer ion/ion reactions of doubly protonated peptides: Effect of elevated bath gas temperature. *Anal. Chem.* **2005**, *77*, 5662–5669.

(4) Gunawardena, H. P.; He, M.; Chrisman, P. A.; Pitteri, S. J.; Hogan, J. M.; Hodges, B. D. M.; McLuckey, S. A. Electron transfer versus proton transfer in gas-phase ion/ion reactions of polyprotonated peptides. *J. Am. Chem. Soc.* **2005**, *127*, 12627–12639.

(5) Gunawardena, H. P.; Gorenstein, L.; Erickson, D. E.; Xia, Y.; McLuckey, S. A. Electron transfer dissociation of multiply protonated and fixed charge disulfide linked polypeptides. *Int. J. Mass. Spectrom.* **2007**, *265*, 130–138.

(6) Zubarev, R. A.; Kelleher, N. L.; McLafferty, F. W. Electron capture dissociation of multiply charged protein cations. A nonergodic process. *J. Am. Chem. Soc.* **1998**, *120*, 3265–3266.

(7) Zubarev, R. A.; Kruger, N. A.; Fridriksson, E. K.; Lewis, M. A.; Horn, D. M.; Carpenter, B. K.; McLafferty, F. W. Electron capture dissociation of gaseous multiply-charged proteins is favored at disulfide

bonds and other sites of high hydrogen atom affinity. *J. Am. Chem. Soc.* **1999**, *121*, 2857−2862.

(8) Zubarev, R. A.; Horn, D. M.; Fridriksson, E. K.; Kelleher, N. L.; Kruger, N. A.; Lewis, M. A.; Carpenter, B. K.; McLafferty, F. W. Electron capture dissociation for structural characterization of multiply charged protein cations. *Anal. Chem.* **2000**, *72*, 563−573.

(9) Zubarev, R. A.; Haselmann, K. F.; Budnik, B.; Kjeldsen, F.; Jensen, R. Towards an understanding of the mechanism of electron-capture dissociation: a historical perspective and modern ideas. *Eur. J. Mass Spectrom.* **2002**, *8*, 337−349.

(10) A recent summary of our work appears in: Simons, J. Analytical model for rates of electron attachment and intramolecular electron transfer in electron transfer dissociation mass spectrometry. *J. Am. Chem. Soc.* **2010**, *132*, 7074−7085.

(11) Syrstad, E. A.; Turecek, F. Hydrogen atom adducts to the amide bond. Generation and energetics of the amino(hydroxy)methyl radical in the gas phase. *J. Phys. Chem. A* **2001**, *105*, 11144−11155.

(12) Turecek, F.; Syrstad, E. A. Mechanism and energetics of intramolecular hydrogen transfer in amide and peptide radicals and cation-radicals. *J. Am. Chem. Soc.* **2003**, *125*, 3353−3369.

(13) Turecek, F.; Polasek, M.; Frank, A.; Sadilek, M. Transient hydrogen atom adducts to disulfides. Formation and energetics. *J. Am. Chem. Soc.* **2000**, *122*, 2361−2370.

(14) Syrstad, E. A.; Stephens, D. D; Turecek, F. Hydrogen atom adducts to the amide bond. Generation and energetics of amide radicals in the gas phase. *J. Phys. Chem. A* **2003**, *107*, 115−126.

(15) Turecek, F. N-C-alpha bond dissociation energies and kinetics in amide and peptide radicals. Is the dissociation a non-ergodic process? *J. Am. Chem. Soc.* **2003**, *125*, 5954−5963.

(16) Syrstad, E. A.; Turecek, F. Toward a general mechanism of electron capture dissociation. *J. Am. Soc. Mass. Spectrom.* **2005**, *16*, 208−224.

(17) Uggerud, E. Electron capture dissociation of the disulfide bond - A quantum chemical model study. *Int. J. Mass. Spectrom.* **2004**, *234*, 45−50.

(18) Anusiewicz, I.; Berdys-Kochanska, J.; Simons, J. Electron attachment step in electron capture dissociation (ECD) and electron transfer dissociation (ETD). *J. Phys. Chem. A* **2005**, *109*, 5801−5813.

(19) Anusiewicz, I.; Berdys-Kochanska, J.; Skurski, P.; Simons, J. Simulating electron transfer attachment to a positively charged model peptide. *J. Phys. Chem. A* **2006**, *110*, 1261−1266.

(20) Sawicka, A.; Skurski, P.; Hudgins, R. R.; Simons, J. Model calculations relevant to disulfide bond cleavage via electron capture influenced by positively charged groups. *J. Phys. Chem. B* **2003**, *107*, 13505−13511.

(21) Sobczyk, M.; Skurski, P.; Simons, J. Dissociative low-energy electron attachment to the C-S bond of H_3CSCH_3 influenced by coulomb stabilization. *Adv. Quantum Chem.* **2005**, *48*, 239−251.

(22) Sawicka, A.; Berdys-Kochanska, J.; Skurski, P.; Simons, J. Low-energy (0.1 eV) electron attachment S-S bond cleavage assisted by coulomb stabilization. *Int. J. Quantum Chem.* **2005**, *102*, 838−846.

(23) Anusiewicz, I.; Berdys, J.; Sobczyk, M.; Sawicka, A.; Skurski, P.; Simons, J. Coulomb-assisted dissociative electron attachment: Application to a model peptide. *J. Phys. Chem. A* **2005**, *109*, 250−258.

(24) Bakken, V.; Helgaker, T.; Uggerud, E. Models of fragmentations induced by electron attachment to protonated peptides. *Eur. J. Mass Spectrom.* **2004**, *10*, 625−638.

(25) Skurski, P.; Sobczyk, M.; Jakowski, J.; Simons, J. Possible mechanisms for protecting NCα bonds in helical peptides from electron-capture (or transfer) dissociation. *Int. J. Mass. Spectrom.* **2007**, *265*, 197−212.

(26) Sobczyk, M.; Neff, D.; Simons, J. Theoretical study of through-space and through-bond electron transfer within positively charged peptides in the gas phase. *Int. J. Mass. Spectrom.* **2008**, *269*, 149−164.

(27) Sobczyk, M.; Simons, J. Distance dependence of through-bond electron transfer rates in electron-capture and electron-transfer dissociation. *Int. J. Mass. Spectrom.* **2006**, *253*, 274−280.

(28) Sobczyk, M.; Simons, J. The role of excited rydberg states in electron transfer dissociation. *J. Phys. Chem. B* **2006**, *110*, 7519−7527.

(29) Neff, D.; Sobczyk, M.; Simons, J. Through-space and through-bond electron transfer within positively charged peptides in the gas phase. *Int. J. Mass Spectrom.* **2008**, *276*, 91−101.

(30) Neff, D.; Simons, J. Theoretical study of electron capture dissociation of $[Mg(H_2O)_n]^{2+}$ clusters. *Int. J. Mass Spectrom.* **2008**, *277*, 166−174.

(31) Turecek, F.; Chen, X.; Hao, C. Where does the electron go? Electron distribution and reactivity of peptide cation radicals formed by electron transfer in the gas phase. *J. Am. Chem. Soc.* **2008**, *130*, 8818−8833.

(32) Chen, X.; Turecek, F. The arginine anomaly: arginine radicals are poor hydrogen atom donors in electron transfer induced dissociations. *J. Am. Chem. Soc.* **2006**, *128*, 12520−12530.

(33) Holm, A. I. S.; Larsen, M. K.; Panja, S.; Hvelplund, P.; Brøndsted Nielsen, S.; Leib, R. D.; Donald, W. A.; Williams, E. R.; Hao, C.; Tureček, F. Electron capture, femtosecond electron transfer and theory: A study of noncovalent crown ether 1,n-diammonium alkane complexes. *Int. J. Mass Spectrom.* **2008**, *276*, 116−126.

(34) Chamot-Rooke, J.; Malosse, C.; Frison, G.; Tureček, F. *J. Am. Soc. Mass Spectrom.* **2007**, *18*, 2146−2161.

(35) Fung, Y. M. E.; Chan, T.-W. D. Experimental and theoretical investigations of the loss of amino acid side chains in electron capture dissociation of model peptides. *J. Am. Soc. Mass Spectrom.* **2005**, *16*, 1523−1535.

(36) Konishi, H.; Yokotake, Y.; Ishibahsia, T. Theoretical study on the electron capture dissociation correlated with proton transfer processes. *J. Mass Spectrom. Soc. Jpn.* **2002**, *50*, 229−232.

(37) Holm, A. I. S.; Hvelplund, P.; Kadhane, U.; Larsen, M. K.; Liu, B.; Nielsen, S. B.; Panja, S.; Pedersen, J. M.; Skryudstrup, T.; Støchkel, K.; Williams, E. R.; Worm, E. S. On the mechanism of electron-capture-induced dissociation of peptide dications from ^{15}N-labeling and crown-ether complexation. *J. Phys. Chem. A* **2007**, *111*, 9641−9643.

(38) Neff, D.; Simons, J. Analytical and computational studies of intramolecular electron transfer pertinent to electron transfer and electron capture dissociation mass spectrometry. *J. Phys. Chem. A* **2010**, *114*, 1309−1323.

(39) Simons, J. Mechanisms for S−S and N−Cα bond cleavage in peptide ECD and ETD mass spectrometry. *Chem. Phys. Lett.* **2010**, *484*, 81−95.

(40) Turecek, F.; Julian, R. R. Peptide radicals and cation radicals in the gas phase. *Chem. Rev.* **2013**, *113*, 6691−6733.

(41) Experimental evidence for SS s* orbitals is given in: Dezarnaud-Dandine, C.; Bournel, F.; Tronc, M.; Jones, D.; Modelli, A. *J. Phys. B* **1998**, *31*, L497−L501. And in: Modelli, A.; Jones, D.; Distefano, G.; Tronc, M. *Chem. Phys. Lett.* **1991**, *181*, 361−366. For amide p* orbitals, see: Seydou, M.; Modelli, A.; Lucas, B.; Konate, K.; Desfrancois, C.; Schermann, J. P. *Eur. Phys. J. D* **2005**, *35*, 199−205 Because the SS s*- and amide p*-attached states have lifetimes in the gas phase in the range $10^{-13}-10^{-14}$ s, they have substantial Heisenberg widths. These widths make specifying precise values for the energies of these states, as they appear in the peptides studied here, impossible. Thus, the energies (1 eV for SS s* and 2.0 eV for amide p*) quoted here should be viewed as estimates with uncertainties in the 0.5−1 eV range..

(42) Neff, D.; Smuczynska, S.; Simons, J. Electron shuttling in electron transfer dissociation. *Int. J. Mass. Spectrom.* **2009**, *283*, 122−134.

(43) Turecek, F.; Chung, T. W.; Moss, C. L.; Wyer, J. A.; Ehlerding, A.; Zettergren, H.; Nielsen, S. B.; Hvelplund, P.; Chamot-Rooke, J.; Bythell, B.; Paizs, B. The histidine effect. Electron transfer and capture cause different dissociations and rearrangements of histidine peptide cation-radicals. *J. Am. Chem. Soc.* **2010**, *132*, 10728−10740.

(44) Moss, C. L.; Chung, T. W.; Wyer, J. A.; Brøndsted Nielsen, S.; Hvelplund, P.; Turecek, F. Dipole-guided electron capture causes abnormal dissociations of phosphorylated pentapeptides. *J. Am. Soc. Mass Spectrom.* **2011**, *22*, 731−751.

(45) Pepin, R.; Laszlo, K. J.; Peng, B.; Marek, A.; Bush, M. F.; Turecek, F. Comprehensive Analysis of Gly-Leu-Gly-Gly-Lys Peptide

7900

dx.doi.org/10.1021/jp5004819 | *J. Phys. Chem. B* 2014, 118, 7892−7901

Dication Structures and Cation-Radical Dissociations Following Electron Transfer; From Electron Attachment to Backbone Cleavage, Ion–Molecule Complexes, and Fragment Separtation. *J. Phys. Chem. A* **2014**, *118*, 308–324.

(46) Hol, W. G. J.; van Duijinen, P. T.; Berendsen, H. J. C. The α-helix dipole and the properties of proteins. *Nature (London)* **1978**, *273*, 443–446.

(47) Sheridan, R. P.; Levy, R. M.; Salemme, F. R. Alpha-helix dipole model and electrostatic stabilization of 4-alpha-helical proteins. *Proc. Natl. Acad. Sci. U. S. A.* **1982**, *79*, 4545–4549.

(48) Stewart, J. J. Optimization of parameters for semiempirical methods V: Modification of NDDO approximations and application to 70 elements. *J. Mol. Model.* **2007**, *13*, 1173–1213.

(49) Stewart, J. J. Application of the PM6 method to modeling the solid state. *J. Mol. Model.* **2008**, *14*, 499–535.

(50) Hudgins, R. R.; Håkansson, K.; Quinn, J. P.; Hendrickson, C. L.; Marshall, A. G. Electron capture dissociation of peptides and proteins does not require a hydrogen atom mechanism. *Proceedings of the 50th ASMS Conference on Mass Spectrometry and Allied Topics*, Orlando, Florida, June 2–6, 2002, A020420 as well as through personal communication to J.S.

(51) Hudgins, R. R.; Jarrold, M. F. Helix Formation in unsolvated alanine-based peptides: helical monomers and helical dimers. *J. Am. Chem. Soc.* **1999**, *121*, 3494–3501.

(52) Schmidt, M. W.; Ruedenberg, K. Effective convergence to complete orbital bases and to the atomic Hartree-Fock limit through systematic sequences of gaussian primitives. *J. Chem. Phys.* **1979**, *71*, 3951–3962.

(53) Simons, J.; Gutowski, M. Double-Rydberg Molecular Anions. *Chem. Rev.* **1991**, *91*, 669–677.

(54) Ditchfield, R.; Hehre, W. J.; Pople, J. A. Self-consistent molecular-orbital methods. IX. An extended gaussian-type basis for molecular-orbital studies of organic molecules. *J. Chem. Phys.* **1971**, *54*, 724–728.

(55) Hehre, W. J.; Ditchfield, R.; Pople, J. A. Self-consistent molecular orbital methods. XII. Further extensions of gaussian-type basis sets for use in molecular orbital studies of organic molecules. *J. Chem. Phys.* **1972**, *56*, 2257–2261.

(56) Hariharan, P. C.; Pople, J. A. Accuracy of AH_n equilibrium geometries by single determinant molecular orbital theory. *Mol. Phys.* **1974**, *27*, 209–214.

(57) Gordon, M. S. The isomers of silacyclopropane. *Chem. Phys. Lett.* **1980**, *76*, 163–168.

(58) Hariharan, P. C.; Pople, J. A. The influence of polarization functions on molecular orbital hydrogenation energies. *Theor. Chim. Acta* **1973**, *28*, 213–222.

(59) Frisch, M. J.; Trucks, G. W.; Schlegel, H. B.; Scuseria, G. E.; Robb, M. A.; Cheeseman, J. R.; Scalmani, G.; Barone, V.; Mennucci, B.; Petersson; et al. *Gaussian 09*, Revision B.01; Gaussian, Inc.: Wallingford, CT, 2009.

(60) Swierszcz, I.; Skurski, P.; Simons, J. Dipole and Coulomb Forces in ECD and ETD Mass Spectroscopy. *J. Phys. Chem. A* **2012**, *116*, 1828–1837.

(61) Boldyrev, A. I.; Simons, J. Theoretical search for large Rydberg molecules: NH_3CH_3, $NH_2(CH_3)_2$, $NH(CH_3)_3$, and $N(CH_3)_4$. *J. Chem. Phys.* **1992**, *97*, 6621–6627.

(62) Holme, A. I. S.; Larsen, M. K.; Panja, S.; Hvelplund, P.; Brønsted-Nielsen, S.; Lieb, R. D.; Donald, W. A.; Williams, E. R.; Hao, C.; Turecek, F. Electron Capture, femtosecond electron transfer and theory; A study of noncovalent crown ether 1,n diammonium alkane complexes. *Int. J. Mass Spectrom.* **2008**, *276*, 116–126.

(63) Hao, C.; Turecek, F. Host-Guest Hydrogen Atom Transfer Induced by Electron Capture. *J. Am. Soc. Mass Spectrom.* **2009**, *20*, 639–651.

(64) In a recent paper, other workers have found that overlap of a Rydberg orbital with an amide p* orbital then allows the electron density to evolve, as the geometry of the electron-attached state relaxes, into a more amide p* dominated state: Turecek, F.; Moss, C. L.; Chung, T. W. Correlating ETD fragment ion intensities with peptide ion conformational and electronic structure. *Int. J. Mass Spectrom.* **2012**, *330–332*, 207–219.

(65) Kohtani, M.; Kinnear, B. S.; Jarrold, M. F. Metal-Ion Enhanced Helicity in the Gas Phase. *J. Am. Chem. Soc.* **2000**, *122*, 12377–12378.